J|A|C|S ARTICLES

Published on Web 06/25/2009

Resonance Chemical Imaging of Polythiophene/Fullerene Photovoltaic Thin Films: Mapping Morphology-Dependent Aggregated and Unaggregated C=C Species

Yongqian Gao and John K. Grey*

Department of Chemistry and Chemical Biology, University of New Mexico, Albuquerque, New Mexico 87131

Received January 26, 2009; E-mail: jkgrey@unm.edu

Abstract: Resonance Raman spectroscopic imaging is introduced as a physical probe to identify and spatially map morphology-dependent variations of intra- and interchain interactions and order in poly-3-hexylthiophene (P3HT) and [6,6]-phenyl-C_{61}-butyric acid methyl ester (PCBM) photovoltaic blend thin films. Absorption spectra and C=C symmetric stretching Raman modes of P3HT/PCBM blend films show contributions from two distinct species that are assigned as aggregated and unaggregated P3HT chains with characteristic Raman frequencies of ~1450 ($I_{C=C}^{agg}$) and ~1470 cm^{-1} ($I_{C=C}^{un}$), respectively. Upon thermal annealing of blend films, the relative concentrations of $I_{C=C}^{agg}$ and $I_{C=C}^{un}$ species ($R = I_{C=C}^{agg}/I_{C=C}^{un}$) changes on average from 0.79 ± 0.20 (as-cast) to 2.45 ± 0.77 (annealed). It is proposed that R values report on the relative densities of states (DOS) of aggregated and unaggregated species, and resonance Raman imaging is then used to spatially map morphology-dependent variations of R values and uncover subclassifications of these species. From both R and frequency dispersion resonance Raman images of $I_{C=C}^{agg}$ and $I_{C=C}^{un}$ species, four distinct types of P3HT chains are identified and mapped in annealed P3HT/PCBM blend thin films: (i) highly aggregated/crystalline, (ii) partially aggregated, (iii) interfacial, and (iv) unaggregated/PCBM rich. The change in aggregation upon annealing is attributed to an increase in planarity of the P3HT chains that is determined from the ratios of C=C/C−C symmetric stretching mode intensities.

Introduction

Morphology-dependent variations of intra- and intermolecular interactions and order in blended photovoltaic donor/acceptor (D/A) thin films have a large impact on the type and densities of electronic states (DOS) and ultimately material performance. Among the most well-studied molecular D/A photovoltaic systems to date are solution processed blends of poly-3-hexylthiophene (P3HT) and [6,6]-phenyl-C_{61}-butyric acid methyl ester (PCBM) that have achieved power conversion efficiencies above 5%.[1−3] These so-called bulk heterojunction systems take advantage of phase segregation between P3HT/PCBM (D/A) components to facilitate charge separation and transport.[4−7] The efficiencies of these processes and that of devices can be enhanced by postprocessing annealing treatments that alter nano- to microscale phase domain size, shape, and composition as well as the DOS of electronic species.[8−12] Unfortunately, reliable control over D/A material morphologies and performance has thus far proven difficult, and only incremental improvements in device efficiencies have been achieved.[13−15] Nevertheless, there are currently intense efforts aimed at controlling the optical and electronic properties of P3HT/PCBM blend thin films by altering film processing conditions (i.e., solvent and temperature),[1,9,16−18] inclusion of additives,[19] and alternative materials deposition and patterning strategies.[20−22]

(1) Ma, W.; Yang, C.; Gong, X.; Lee, K.; Heeger, A. J. *Adv. Funct. Mater.* **2005**, *15*, 1617–1622.
(2) Kim, Y.; Cook, S.; Tuladhar, S. M.; Choulis, S. A.; Nelson, J.; Durrant, J. R.; Bradley, D. D. C.; Giles, M.; McCulloch, I.; Ha, C.-S.; Ree, M. *Nat. Mater.* **2006**, *5*, 197–203.
(3) Reyes-Reyes, M.; Kim, K.; Carroll, D. L. *Appl. Phys. Lett.* **2005**, *87*, 083506/1−083506/3.
(4) Yu, G.; Gao, J.; Hummelen, J. C.; Wudl, F.; Heeger, A. J. *Science* **1995**, *270*, 1789–1791.
(5) Coakley, K. M.; McGehee, M. D. *Chem. Mater.* **2004**, *16*, 4533–4542.
(6) Sariciftci, N. S.; Smilowitz, L.; Heeger, A. J.; Wudl, F. *Science* **1992**, *258*, 1474–1476.
(7) Halls, J. J. M.; Walsh, C. A.; Greenham, N. C.; Marseglia, E. A.; Friend, R. H.; Moratti, S. C.; Holmes, A. B. *Nature* **1995**, *376*, 498–500.
(8) Shaheen, S. E.; Brabec, C. J.; Sariciftci, N. S.; Padinger, F.; Fromherz, T.; Hummelen, J. C. *Appl. Phys. Lett.* **2001**, *78*, 841–843.
(9) Li, G.; Shrotriya, V.; Huang, J.; Yao, Y.; Moriarty, T.; Emery, K.; Yang, Y. *Nat. Mater.* **2005**, *4*, 864–868.
(10) Camaioni, N.; Ridolfi, G.; Casalbore-Miceli, G.; Possamai, G.; Maggini, M. *Adv. Mater.* **2002**, *14*, 1735–1738.
(11) Campoy-Quiles, M.; Ferenczi, T.; Agostinelli, T.; Etchegoin, P. G.; Kim, Y.; Anthopoulos, T. D.; Stavrinou, P. N.; Bradley, D. D. C.; Nelson, J. *Nat. Mater.* **2008**, *7*, 158–164.
(12) Ayzner, A. L.; Wanger, D. D.; Tassone, C. J.; Tolbert, S. H.; Schwartz, B. J. *J. Phys. Chem. C* **2008**, *112*, 18711–18716.
(13) Scharber, M. C.; Muehlbacher, D.; Koppe, M.; Denk, P.; Waldauf, C.; Heeger, A. J.; Brabec, C. J. *Adv. Mater.* **2006**, *18*, 789–794.
(14) Guenes, S.; Neugebauer, H.; Sariciftci, N. S. *Chem. Rev.* **2007**, *107*, 1324–1338.
(15) Thompson, B. C.; Frechet, J. M. J. *Angew. Chem., Intl. Ed.* **2008**, *47*, 58–77.
(16) Li, G.; Yao, Y.; Yang, H.; Shrotriya, V.; Yang, G.; Yang, Y. *Adv. Funct. Mater.* **2007**, *17*, 1636–1644.
(17) Li, G.; Shrotriya, V.; Yao, Y.; Yang, Y. *J. Appl. Phys.* **2005**, *98*, 043704/1−043704/5.
(18) Li, G.; Shrotriya, V.; Yao, Y.; Huang, J.; Yang, Y. *J. Mater. Chem.* **2007**, *17*, 3126–3140.

10.1021/ja900636z CCC: $40.75

Finding the optimal functional form of P3HT/PCBM systems is therefore of great practical importance, which can only be realized from the aid of sensitive physical probes capable of correlating local structure to material performance.

To this end, spectroscopic or surface probe techniques are frequently combined with device current−voltage ($I-V$) or photocurrent action spectra to report on material structural changes arising from variable processing conditions on P3HT/PCBM performance in a functioning device.[11,14,23−25] Optical spectroscopic studies of P3HT/PCBM films have shown marked changes in both the type and DOS of electronic species depending on processing conditions and postprocessing annealing treatments. For example, P3HT/PCBM blend films cast from low boiling point solvents, such as chloroform, generally yield broad and overlapping absorption transitions with little or no resolved vibronic structure.[16,26−28] Device $I-V$ curves from these 'as-cast' films likewise show lower current densities and device efficiencies (<1%). Upon annealing, spectra recover resolved vibronic structure in the dominant C═C symmetric stretching mode, which is commonly attributed to increased ordering (crystallinity) of the P3HT component, resulting in improved device current densities and efficiencies (>5%).[11]

Interestingly, recent spectroscopic studies on undoped P3HT thin films have demonstrated that the lowest energy optical absorption band is non-Poissonian and consists of overlapping transitions from both *intrachain* (unaggregated) and *interchain* (aggregated) species.[29−31] The presence of two distinct P3HT species has also been confirmed from recent electronic structure calculations showing the existence of both crystalline (aggregated) and amorphous (unaggregated) forms with an energy difference of ∼0.25 eV (2015 cm^{-1}), in good agreement with experiment.[32] In P3HT/PCBM blends, the nature of P3HT intra- and interchain interactions is more complex since the degree of phase segregation between both components affects these interactions differently than the undoped polymer. Moreover, these interactions are modulated by morphological heterogeneity, thus affecting the relative DOS of both aggregated and unaggregated species that, while having a profound impact on material performance, remains poorly understood. We herein propose an extension to the physical picture developed from undoped P3HT films to describe the morphology-dependent relative DOS of aggregated and unaggregated species in P3HT/PCBM blend thin films.

Resonance Raman spectroscopy and imaging is introduced in the following that has much higher spatial resolution and chemical sensitivity than conventional optical absorption spectroscopy techniques enabling a detailed study of morphological heterogeneity on aggregated and unaggregated species. The noninvasive nature, strong resonance enhancements of Franck−Condon displaced modes, and suppressed fluorescence backgrounds due to charge transfer quenching make Raman techniques highly amenable for studying local ground and excited state structure of photovoltaic polymeric blend systems.[28,34−36,38,40] Several groups have in fact used Raman spectroscopy to track changes in the characteristic C═C symmetric stretching backbone mode of P3HT in P3HT/PCBM blend thin films upon annealing to establish a correlation between chemical structure and device performance.[34,38,39] For example, Raman spectroscopic studies of as-cast P3HT/PCBM blend thin films reveal unusually broad C═C bands with maxima at ∼1462 cm^{-1}.[40] Upon annealing, this band shifts to ∼1448 cm^{-1}, narrows, and becomes virtually indistinguishable from that of undoped P3HT.[40] Although the phenomenological trends in P3HT C═C Raman band frequency shifts and line shape serve as a reliable reporter for correlating local structure to material performance, the physical origins of these effects are not entirely straightforward. Upon closer inspection, the P3HT C═C line shape shows significant deviations from an idealized Lorentzian line shape, i.e., overlapping transitions or shoulders, suggesting contributions from more than one species. It is demonstrated here that the C═C band of P3HT actually consists of two components centered at ∼1450 cm^{-1} ($I_{C=C}^{agg}$) and ∼1470 cm^{-1} ($I_{C=C}^{un}$), and changes in their relative concentrations upon annealing leads to apparent spectral shifts and overall line shape changes. These two C═C components are assigned as aggregated ($I_{C=C}^{agg}$) and unaggregated ($I_{C=C}^{un}$) P3HT species that show, on average, changes in relative concentrations ($I_{C=C}^{agg}/I_{C=C}^{un}$ ratios, R) from 0.79 ± 0.20 to 2.45 ± 0.77 between as-cast and annealed P3HT/PCBM films, respectively. For longer annealing times of blend films, R values observed in undoped P3HT thin films are recovered (∼5.5), suggesting complete phase segregation of both P3HT/PCBM components. On the basis of similar trends in ensemble absorption spectra of as-cast and annealed blend films, it is proposed that the R values measured from resonance Raman spectroscopy can be used as a reporter of the relative DOS of aggregated and unaggregated species in the P3HT component in blend films. Resonance Raman spectroscopic imaging is then used to spatially map morphology-dependent R values for both as-cast and annealed films to reveal the landscapes of the morphology-dependent relative DOS in P3HT/PCBM composite blend thin films. Frequency dispersion maps of $I_{C=C}^{agg}$ and $I_{C=C}^{un}$ species are also generated that, together with R images, allow us to assign

(19) Lee, J. K.; Ma, W. L.; Brabec, C. J.; Yuen, J.; Moon, J. S.; Kim, J. Y.; Lee, K.; Bazan, G. C.; Heeger, A. J. *J. Am. Chem. Soc.* **2008**, *130*, 3619–3623.
(20) Xin, H.; Kim, F. S.; Jenekhe, S. A. *J. Am. Chem. Soc.* **2008**, *130*, 5424–5425.
(21) Lee, S. H.; Park, D. H.; Kim, K.; Joo, J.; Kim, D.-C.; Kim, H.-J.; Kim, J. *Appl. Phys. Lett.* **2008**, *91*, 263102/1–263102/3.
(22) Li, L.; Lu, G.; Yang, X. *J. Mater. Chem.* **2008**, *18*, 1984–1990.
(23) Coffey, D. C.; Ginger, D. S. *Nat. Mater.* **2006**, *5*, 735–740.
(24) Coffey, D. C.; Reid, O. G.; Rodovsky, D. B.; Bartholomew, G. P.; Ginger, D. S. *Nano Lett.* **2007**, *7*, 738–744.
(25) Dante, M.; Peet, J.; Nguyen, T.-Q. *J. Phys. Chem. C* **2008**, *112*, 7241–7249.
(26) Nguyen, L. H.; Hoppe, H.; Erb, T.; Guenes, S.; Gobsch, G.; Sariciftci, N. S. *Adv. Funct. Mater.* **2007**, *17*, 1071–1078.
(27) Sohn, Y.; Stuckless, J. T. *Appl. Phys. Lett.* **2007**, *90*, 171901/1–171901/3.
(28) Miller, S.; Fanchini, G.; Lin, Y.-Y.; Li, C.; Chen, C.-W.; Su, W.-F.; Chhowalla, M. *J. Mater. Chem.* **2008**, *18*, 306–312.
(29) Spano, F. C. *Chem. Phys.* **2006**, *325*, 22–35.
(30) Manas, E. S.; Spano, F. C. *J. Chem. Phys.* **1998**, *109*, 8087–8101.
(31) Clark, J.; Silva, C.; Friend, R. H.; Spano, F. C. *Phys. Rev. Lett.* **2007**, *98*, 206406/1–206406/4.
(32) Vukmirovic, N.; Wang, L.-W. *J. Phys. Chem. B* **2009**, *113*, 409–415.
(33) Casado, J.; Hicks, R. G.; Hernandez, V.; Myles, D. J. T.; Ruiz Delgado, M. C.; Lopez Navarrete, J. T. *J. Chem. Phys.* **2003**, *118*, 1912–1920.
(34) Yun, J.-J.; Peet, J.; Cho, N.-S.; Bazan, G. C.; Lee, S. J.; Moskovits, M. *Appl. Phys. Lett.* **2008**, *92*, 251912/1–251912/3.
(35) Milani, A.; Brambilla, L.; Zoppo, M. D.; Zerbi, G. *J. Phys. Chem. B* **2007**, *111*, 1271–1276.
(36) Bruevich, V. V.; Makhmutov, T. S.; Elizarov, S. G.; Nechvolodova, E. M.; Paraschuk, D. Y. *J. Chem. Phys.* **2007**, *127*, 104905/1–104905/9.
(37) Liao, Z.; Pemberton, J. E. *J. Phys. Chem. A* **2006**, *110*, 13744–13753.
(38) Bao, Q.; Gan, Y.; Li, J.; Li, C. M. *J. Phys. Chem. C* **2008**, *112*, 19718–19726.
(39) Klimov, E.; Li, W.; Yang, X.; Hoffmann, G. G.; Loos, J. *Macromolecules* **2006**, *39*, 4493–4496.
(40) Janssen, G.; Aguirre, A.; Goovaerts, E.; Vanlaeke, P.; Poortmans, J.; Manca, J. *Eur. Phys. J.: Appl. Phys.* **2007**, *37*, 287–290.

subclassifications and identify spatial distributions of these species within the blend films. The degree of aggregation measured from *R* values and images is attributed to the planarity of the P3HT chains that can be inferred from changes in the relative intensities of the C−C symmetric stretching vibration (∼1380 cm^{-1}). Upon annealing, the intensities of these modes increase by about a factor of 2, and by constructing images of the ratio of C═C and C−C backbone stretching mode Raman intensities ($I_{C=C}/I_{C-C}$) we find that regions of high aggregation (high *R* values) are well correlated to regions of greater planarity (small $I_{C=C}/I_{C-C}$ values).

We conclude by briefly discussing the possible implications of P3HT aggregation on charge transfer processes in device structures and suggest future experiments to directly correlate *R* values to photocurrent generation efficiencies. Overall, the information content afforded from this resonance Raman imaging approach provides a new insight into the impact of morphological heterogeneity on the relative DOS of aggregated and unaggregated P3HT chains in blend films that can aid materials scientists in the development of new processing strategies for improved material performance in photovoltaic devices.

Experimental Section

Materials and Sample Preparation. Electronic grade, regioregular poly-3-hexylthiophene (P3HT, $M_n \approx 87\,000$ g/mol) and [6,6]-phenyl-C_{61}-butyric acid methyl ester (PCBM) were purchased from Rieke metals and Aldrich, respectively, and used without further purification. Materials were dissolved in either chlorobenzene (CB) or toluene at a concentration of 10 mg/mL for ∼12 h and filtered using a 0.2 μm filter (Whatman) to remove any undissolved solid. Glass coverslips were used as substrates that were rigorously cleaned by sonication in trichloroethylene, acetone, and methanol each for 15 min. Blend thin films were deposited by spin casting solutions of a 1:1 w/w ratio of P3HT/PCBM at speeds of 1000 rpm for 80 s, resulting in a ∼80 nm thick film verified by atomic force microscopy (AFM). Postprocessing thermal annealing treatments were used to control the morphologies of blend films by heating samples on a hot plate at 130 °C for 20 min in a N_2 environment. Thin films were then coated with aluminum (∼70 nm) by thermal vapor deposition under high vacuum to prevent degradation from oxygen and moisture.

Instrumentation. Optical absorption spectra of unsealed blend films were recorded on a UV/vis spectrometer (Varian CARY 1C) in a scan range from 300 to 800 nm. Raman spectra and images were recorded using a home-built microscope spectrometer equipped with a nanopositioning stage (Madcity, Nano-View/M-XY) and electron multiplying CCD camera (Andor Newton). A multicolor laser source (Ar/Kr ion, laser wavelengths range from 476 to 676 nm) was used to excite the sample at different wavelengths across the P3HT absorption spectrum (488, 568, and 647 nm). The unpolarized laser beam was directed into the microscope, reflected by a multicolor dichroic filter, and focused to a diffraction limited spot by an oil immersion objective (Zeiss plan-apochromat, NA = 1.4). Raman edge filters (Semrock) were used to remove Rayleigh-scattered excitation light, and Raman-scattered light was focused onto the entrance slits of a single-stage polychromator (Andor Shamrock 303i), dispersed by a 1800 line/mm holographic grating and imaged onto the CCD. Typical spectral acquisition times were ∼200 ms to 1s, and excitation intensities were $\sim 10^5$ W/cm^2 for all excitation wavelengths used. Instrument resolution was 2 cm^{-1}, and experimental line widths did not vary with the choice of slit width. Raman spectra of both as-cast and annealed films were corrected for the reabsorption of scattered light using the procedure described in ref 41, which resulted in minor changes in intensities (∼4%) and no changes in line shapes. Photodegradation studies of sealed thin films show no noticeable time-dependent behavior for acquisition periods >100× longer than that used in this work beyond random intensity fluctuations due to shot noise (see Supporting Information). Raman images were generated by raster scanning the nanopositioning stage over the laser spot in a synchronous fashion with CCD spectral acquisition using a LABVIEW program. Images were scanned for $N \times N$ points, where N is the number of points per line and scan ranges varied from ∼10 to 100 μm based on the sizes of P3HT/PCBM phase-segregated domains determined from AFM measurements. Raman images were processed using a homemade program by plotting either the integrated intensity (area), frequency, or line width of a particular Raman band for each spectrum at each scan position. Spectral deconvolution of overlapping Raman bands was accomplished by performing a least-squares analysis using Lorentzian functions with fixed line widths and frequency ranges.

Results and Discussion

Previous reports of absorption spectra from undoped P3HT thin films show non-Poissonian line shapes that can be decomposed into contributions from interchain (aggregated) and intrachain (unaggregated) species.[29,31,42] Weakly coupled H-aggregate (interchain) species comprise the lowest energy transitions that exhibit resolved vibronic structure due to their highly ordered or quasi-crystalline nature and increased conjugation lengths.[29,31] In contrast, unaggregated (intrachain) species show broadened and blue-shifted bands similar to dilute solution spectra, suggesting substantial disorder and reduced conjugation lengths.[31] The physical basis for the assignment of the red-shifted species as H aggregates arises from the fact that the P3HT chains adopt a more planar conformation, thus leading to longer conjugation lengths and hence lower transition energies. Unaggregated P3HT molecules, on the other hand, are believed to exist in a more twisted conformation, and therefore, conjugation lengths are reduced, leading to blue shifted band maxima.[42,43] In P3HT/PCBM blend films, intra- and interchain interactions and, therefore, the relative DOS of aggregated and unaggregated P3HT species depend primarily on the degree of phase segregation between these components that, in turn, depends on the solvent characteristics and postprocessing annealing treatments. In this paper, we extend the physical picture borne out of absorption spectroscopic and theoretical studies of chain packing interactions in undoped P3HT thin films to elucidate the morphology-dependent variations of the relative DOS of aggregated and unaggregated species in P3HT/PCBM blend thin films.

We first consider electronic absorption line shapes of P3HT/PCBM thin films in order to understand the basic nature of the relative DOS of aggregated and unaggregated species and their dependence on postprocessing annealing treatments. Figure 1a and 1b presents absorption spectra of P3HT/PCBM blend thin films cast from chlorobenzene (a) and thermally annealed films (b) focusing on the P3HT region (∼14 500−25 000 cm^{-1}). Although optical absorption spectra of P3HT/PCBM blends are intrinsically more complex than those of undoped P3HT, no significant evidence for ground state charge transfer interactions exists (i.e., broad, overlapping, and red-shifted bands); thus, blend spectra can be described by a linear superposition of single

(41) Shriver, D. F.; Dunn, J. B. R. *Appl. Spectrosc.* **1974**, *28*, 319–323.
(42) Brown, P. J.; Thomas, D. S.; Kohler, A.; Wilson, J. S.; Kim, J.-S.; Ramsdale, C. M.; Sirringhaus, H.; Friend, R. H. *Phys. Rev. B* **2003**, *67*, 064203/1−064203/16.
(43) Koren, A. B.; Curtis, M. D.; Francis, A. H.; Kampf, J. W. *J. Am. Chem. Soc.* **2003**, *125*, 5040–5050.

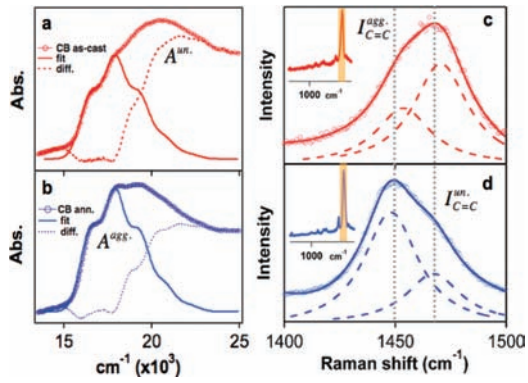

Figure 1. Absorption spectra of as-cast (a, red) and annealed (b, blue) P3HT/PCBM blend thin films (circles). The structured onsets of both absorption spectra are fitted using a literature model that accounts for aggregation effects on the 0−0 transition (A^{agg}, solid trace).[29] Fits are then subtracted from experimental spectra, revealing a broad, higher energy band corresponding to unaggregated segments of P3HT (A^{un}, dashed trace). Raman spectra of as-cast (c, red) and annealed (d, blue) blend films excited with 488 nm (20 492 cm^{-1}) light show the P3HT C═C symmetric stretching band represented by the shaded regions of the complete spectra shown as insets in c and d. The C═C mode is fitted with two Lorentzian functions (dashed traces) of the form $y_1 + A_1\{\Gamma^2/[(x - x_1)^2 + \Gamma^2]\} + y_2 + A_2\{\Gamma^2/[(x - x_2)^2 + \Gamma^2]\}$, showing the relative contributions of both aggregated ($I_{C=C}^{agg}$) and unaggregated ($I_{C=C}^{un}$) components (see text for details).

P3HT and PCBM component spectra. Qualitative comparison of experimental spectra in Figure 1a and 1b reveals that marked changes in both line shape and maxima occur upon annealing that are typically rationalized in terms of competing intra- and interchain interactions and ordering effects within the P3HT component.[18]

A vibronic analysis of P3HT/PCBM as-cast and annealed absorption spectra is performed to unravel the contributions of both aggregated and unaggregated species to the total P3HT/PCBM absorption line shape. In these simulations, the low-energy, structured onset region (i.e., H-aggregate portion) is fitted for both as-cast and annealed spectra using a single Franck−Condon progression in the excited state P3HT C═C symmetric stretching vibrational frequency (∼1400 cm^{-1}) (solid traces, Figure 1a and 1b). Fit spectra are calculated using a model described in ref 29 that accounts for aggregation effects, i.e., reduced intensity of the 0−0 transition which can become allowed due to disorder effects. Both as-cast and annealed absorption spectra can be fitted using the same energy of electronic origin (E_{00}) of 16 500 cm^{-1}, while line widths of individual vibronic transitions are slightly broader for the former (fwhm, 810 vs 840 cm^{-1}). As seen in previous electronic absorption studies of undoped P3HT thin films, a single Franck−Condon progression is not sufficient to fit either spectrum. By subtracting the fitted spectrum, a broad and blue-shifted spectrum emerges similar to that of a dilute (<0.001 wt %) P3HT/PCBM solution spectrum (see Supporting Information). This feature has also been observed in polarized ellipsometry studies of undoped polythiophenes whereby the out-of-plane component of the optical dielectric constant shows a blue-shifted and broad line shape.[44] On the basis of previous observations in undoped P3HT, the lower energy, structured spectrum is assigned as a weakly coupled H-aggregate species (A^{agg}) and the higher energy, broadened spectra correspond to transitions from unaggregated P3HT chains (A^{un}).

It is interesting to note that both the energies and line shapes of the A^{agg} spectrum change relatively little with annealing, i.e., similar C═C dimensionless normal coordinate offsets ($\Delta_{annealed}$ = 1.3 vs $\Delta_{as\text{-}cast}$ = 1.4), which suggests that the nature of interchain interactions ($\pi-\pi$ stacking) does not change. Estimates of excited state displacements for the A^{un} portion of the overall spectrum are obtained from the band width that yield an effective Δ value of ∼3. The large differences in Δ values for the aggregated and unaggregated species are likely the result of large displacements in the low-frequency torsional vibrations (∼200−400 cm^{-1}) in the latter in addition to contributions from the C═C mode. These estimates provide further insight into the geometric properties of both P3HT excited species, namely, smaller Δ values and resolved line shapes in aggregates suggest a planar conformation and longer conjugation lengths, whereas the broad and unresolved line shapes of unaggregated species indicate a twisted conformation, leading to shorter conjugation lengths. On the basis of the small change in Δ for the A^{agg} portion of both as-cast and annealed films, lack of ground state charge transfer interactions, and overall similarity to undoped P3HT absorption spectra,[31] we conclude that PCBM molecules mainly modulate P3HT intra- and interchain interactions in blend films and therefore the relative DOS of aggregated and unaggregated species. Estimates of the relative DOS parameter are now determined by taking the ratios of integrated line shapes for aggregated and unaggregated bands (i.e., A^{agg}/A^{un}) that yield values of ∼0.53 and ∼1.2 for as-cast and annealed films, respectively. It is important to note that these estimates are qualitative in nature due to the different Franck−Condon normal coordinate contributions and displacements for both transitions. Moreover, these values represent the average over the entire film, thereby masking effects of morphological heterogeneity, which cannot be resolved by conventional absorption spectroscopic techniques. To overcome these limitations, resonance Raman spectroscopy and imaging is used to report on morphology-dependent variations in the relative DOS of aggregated/unaggregated species in as-cast and annealed P3HT/PCBM thin films.

Previous reports of P3HT/PCBM Raman spectra have shown broad and overlapping C═C symmetric stretching mode line shapes that exhibit large red shifts (>15 cm^{-1}) and narrowing upon annealing or casting films from high boiling point solvents.[34,40] These effects are generally rationalized as a single C═C band that gradually narrows and shifts to lower frequencies due to increased intra- and interchain order and conjugation lengths.[28,34,40] We now delve further into the physical origins of these effects by first considering the characteristics of Raman line shapes for both as-cast and annealed films. Figure 1c and 1d shows Raman spectra of as-cast (c) and annealed (d) P3HT/PCBM thin films in the P3HT C═C symmetric stretching mode region excited on resonance with both the aggregated and unaggregated absorption transitions of the P3HT component at 488 nm (20 492 cm^{-1}). The complete spectra are shown as insets with colored bars highlighting the C═C band that are much simpler than spectra excited off resonance[28] due to large enhancements of the P3HT C═C backbone mode scattering cross sections. Raman spectra of pure PCBM films excited under the same conditions showed negligible Raman intensities, similar to previous Raman studies of P3HT/PCBM films,[34,39,40,45] and we therefore rule out any contributions from this component to the P3HT C═C line shape (see Supporting Information). Upon

(44) Gurau, M. C.; Delongchamp, D. M.; Vogel, B. M.; Lin, E. K.; Fischer, D. A.; Sambasivan, S.; Richter, L. J. *Langmuir* **2007**, *23*, 834–842.

(45) Malgas, G. F.; Arendse, C. J.; Mavundla, S.; Cummings, F. R. *J. Mater. Sci.* **2008**, *43*, 5599–5604.

closer inspection of the C═C Raman band for both as-cast and annealed films it is apparent that these line shapes consist of at least two overlapping transitions. Furthermore, previous Raman spectroscopic studies of polythiophenes demonstrate that this band does not split with alkyl substitution on the 3 position of the thiophene ring,[46] thus qualitatively confirming the origin of this irregular line shape as two different C═C species arising from different local environments. A least-squares procedure is used to fit two Lorentzian components (dashed traces, Figure 1c and 1d) to uncover the contributions of these species to the total line shape. To ensure unique and reliable fits, line widths were kept constant (15 cm^{-1}) and center frequencies of both species (~1450 cm^{-1} and ~1470 cm^{-1}, respectively) were constrained within 0.5% of the average center frequency (approximately ±5 cm^{-1}). The choice of line widths for these two species was determined by varying Lorentzian fit line widths and comparing residuals which yielded best average values of 15 ± 1 cm^{-1} (see Supporting Information). There was also no dependence of the fitted center frequency on the initial guess in our fit procedure when this parameter was varied within the above range (see Supporting Information). On the other hand, amplitudes were allowed to vary, which reflects the morphology-dependent concentrations of both C═C species.

Herein, spectral shifts and line shape changes in the P3HT C═C mode upon annealing are described in terms changes in the relative concentrations of the C═C mode components due to alterations in P3HT packing interactions and order. From both experimental absorption spectroscopy and theoretical studies of undoped P3HT, the P3HT/PCBM blend lower frequency component is assigned as aggregated P3HT C═C species ($I_{C=C}^{agg}$) and the higher frequency component is assigned as unaggregated P3HT C═C species ($I_{C=C}^{un}$). In this scheme, $I_{C=C}^{agg}$ species represent P3HT chains with larger intra- and interchain order or H-aggregate-like with longer conjugation lengths whereas $I_{C=C}^{un}$ species correspond to chains with lower intra- and interchain order or unaggregated P3HT chains and shorter conjugation lengths. This assignment is also supported by recent theoretical and experimental studies on oligothiophenes that exhibit similar trends in Raman frequencies due to competing intra- and interchain ordering effects.[35]

Assuming that Raman scattering cross sections of both $I_{C=C}^{agg}$ and $I_{C=C}^{un}$ components do not change throughout the films, the ratio, R, of Raman intensities of both components is taken to obtain the relative concentrations ($N_{C=C}$) of aggregated and unaggregated species:

$$R = \frac{I_{C=C}^{agg}}{I_{C=C}^{un}} \approx \frac{N_{C=C}^{agg}}{N_{C=C}^{un}} \quad (1)$$

As-cast films had average R values of ~0.8, whereas annealed films have ratios of ~2. On the basis of similar trends of the relative aggregated/unaggregated DOS from absorption spectra of as-cast and annealed films, it is proposed that R values measured from resonance excitation can be used as a reporter for the relative aggregated/unaggregated DOS in P3HT/PCBM photovoltaic thin films. Because no structural relaxation effects occur in the Raman process, the R values are expected to provide a more meaningful and reliable estimate of the relative DOS compared to absorption bands. We now extend our resonance Raman spectroscopic approach to perform hyperspectral imaging and spatially map morphology-dependent R values and frequency dispersion of $I_{C=C}^{agg}$ and $I_{C=C}^{un}$ species for both as-cast and annealed P3HT/PCBM blend thin films.

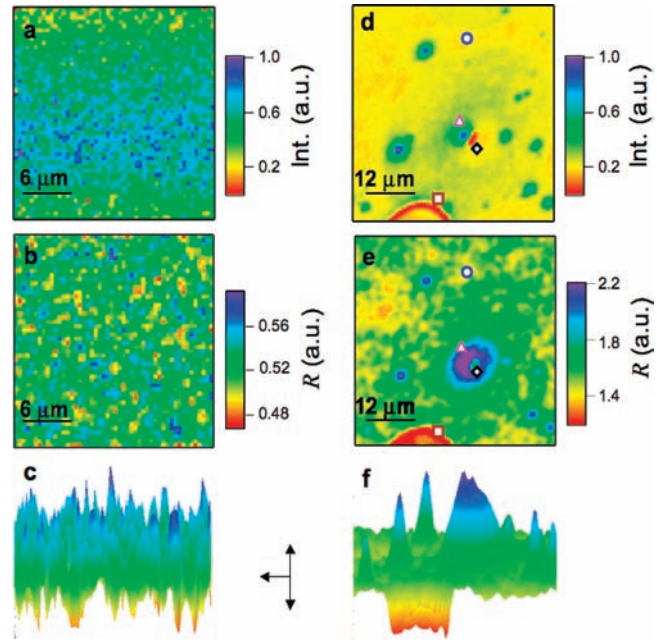

Figure 2. Normalized resonance Raman images of the total integrated intensity and ratio images of Lorentzian components (R) of the C═C symmetric stretching mode of as-cast (a and b) and annealed (d and e) P3HT/PCBM thin films, respectively. Surface contour plots of R images for as-cast and annealed films are shown in panels c and f, respectively.

Resonance Raman imaging measurements performed on three different samples yielded average R values of 0.79 ± 0.20 and 2.45 ± 0.77 for as-cast and annealed films, respectively. Additionally, the average frequencies of $I_{C=C}^{agg}$ species were found to be 1452 ± 2.6 and 1449 ± 1.4 cm^{-1} for as-cast and annealed films, respectively, whereas $I_{C=C}^{un}$ species for both types of films had average values of 1471 ± 1.0 cm^{-1}. Despite sample-to-sample heterogeneity effects, as-cast and annealed films showed similar trends, and these characteristics are discussed in detail in the following using representative as-cast and annealed films prepared from the same blend solution. Figure 2a and 2d presents resonance Raman images of the C═C symmetric stretching mode normalized total integrated intensities of representative as-cast and annealed P3HT/PCBM blend thin films. Because the size scale of P3HT/PCBM phase segregation determined from AFM is below the lateral resolution of our instrument, it is not possible to comment on features observed in as-cast Raman images. On the contrary, annealed films show rich structure owing to the phase-segregated nature of P3HT/PCBM components on the >1 μm size scale that is easily resolved by our apparatus. Overall, our Raman images exhibit similar features as observed in TEM,[47] electro-force microscopy,[25] and off-resonance excitation Raman imaging[39] studies of P3HT/PCBM blend thin films. However, the principal advantage of our approach is the ability to spatially resolve the morphology-dependent variation of the relative DOS of $I_{C=C}^{agg}$ and $I_{C=C}^{un}$ species. R images of representative of as-cast and annealed blend thin films are presented in Figure 2b and 2e, revealing the impact of local morphology and packing interac-

(46) Louarn, G.; Trznadel, M.; Buisson, J. P.; Laska, J.; Pron, A.; Lapkowski, M.; Lefrant, S. *J. Phys. Chem.* **1996**, *100*, 12532–12539.

(47) Vanlaeke, P.; Swinnen, A.; Haeldermans, I.; Vanhoyland, G.; Aernouts, T.; Cheyns, D.; Deibel, C.; D'Haen, J.; Heremans, P.; Poortmans, J.; Manca, J. V. *Sol. Energy Mater. Sol. Cells* **2006**, *90*, 2150–2158.

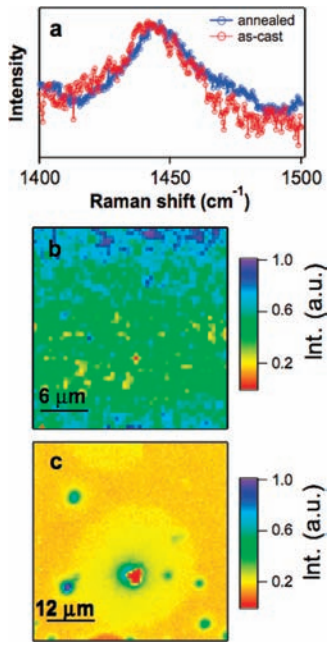

Figure 3. (a) Typical Raman spectra of as-cast and annealed P3HT/PCBM thin films excited with 647 nm light in the P3HT C═C stretching mode region. (b and c) Normalized Raman intensity images measured at the same region as Figure 2a and 2d for as-cast and annealed films, respectively.

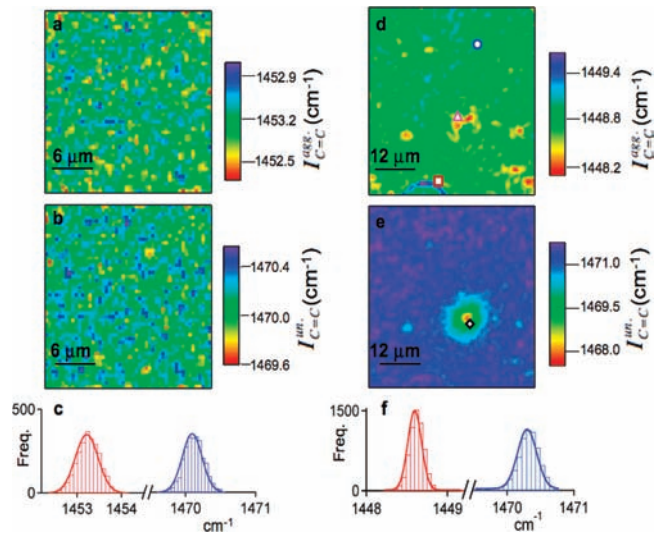

Figure 4. (a and b) $I_{C=C}^{agg}$ and $I_{C=C}^{un}$ center frequency dispersion images for P3HT/PCBM as-cast films, and (c) histograms of frequency components. (d and e) $I_{C=C}^{agg}$ and $I_{C=C}^{un}$ center frequency images for P3HT/PCBM annealed films, and (f) histograms of frequency components. Symbols are superimposed which correspond to the same regions as shown in Figure 2c and 2d.

tions on intra- and interchain order. The as-cast film had an average R value of 0.52 ± 0.02, suggesting a greater number of $I_{C=C}^{un}$ species and implying highly interspersed P3HT/PCBM molecules that largely suppress interchain aggregate formation. The annealed film, on the other hand, had an average R value of 1.71 ± 0.07, revealing a greater number of $I_{C=C}^{agg}$ species due to increased phase segregation. Surface contour plots of both as-cast and annealed films, respectively, are shown in Figure 2c and 2f, which provides greater detail into the morphology-dependent distributions of both C═C species.

In order to compare excitation wavelength effects, Raman spectra and images were also measured under off-resonance conditions using 647 nm (15 455 cm^{-1}), which is expected to selectively excite $I_{C=C}^{agg}$ species due to preresonance enhancement effects. Figure 3a shows Raman spectra of the C═C symmetric stretching mode region of as-cast and annealed P3HT/PCBM blend thin films as well as normalized intensity images measured for the same region as shown previously for 488 nm excitation, Figure 3b and 3c, respectively. Since 647 nm excitation should not excite $I_{C=C}^{un}$ species, significant deviations from the line shapes presented in Figure 1c and 1d are expected. Indeed, both as-cast and annealed films excited off-resonance exhibit broadened Raman line shapes and average frequencies of ∼1444 cm^{-1}, which represents a substantial red shift compared to either $I_{C=C}^{agg}$ or $I_{C=C}^{un}$ center frequencies measured at 488 nm. It is also important to note that increased background fluorescence in off-resonance spectra leads to diminished signal-to-noise ratios, especially for annealed films which have higher P3HT fluorescence yields presumably due to reduced charge transfer quenching. The lack of dependence of P3HT C═C Raman line shapes with thin film processing conditions for off-resonance excitation conditions is most likely the result of selective enhancement of minority $I_{C=C}^{agg}$ species with long conjugation lengths. In this limit it is not possible to compare R values since both aggregated and unaggregated species are not excited equally; therefore, off-resonance excitation is not a reliable means to interrogate morphology-dependent variations in the relative DOS of aggregated/unaggregated species.

Further comparison of normalized integrated intensity and R images for the annealed film resonance Raman image reveals four distinct regions, represented by the symbols in Figure 2d and 2e that represent distinct subclassifications of aggregated and unaggregated P3HT species. Black diamonds highlight regions with low Raman intensities (<0.2) and $R < 1$, blue circles represent regions of intermediate intensities ($0.2 < I < 0.6$) and $1 < R < 1.5$, and purple triangles correspond to high intensities (>0.6) with R >1.5. Additionally, the P3HT/PCBM phase-segregated domain size scales are larger than our instrument resolution (∼210 nm), making it possible to interrogate the interface region between both components, which is represented by brown squares. However, due to the direct correspondence between intensity and R images, these maps are not sufficient to assign the possible structural origins of these features. We instead rely on frequency dispersion maps of $I_{C=C}^{agg}$ and $I_{C=C}^{un}$ species that provide greater insight into the identity and morphology-dependent distributions of these species throughout the films.

As-cast film frequency dispersion images of $I_{C=C}^{agg}$ and $I_{C=C}^{un}$ species are shown in Figure 4a and 4b, and those of the annealed film are shown in Figure 4d and 4e. Histograms of these frequencies are also included in Figure 4c and 4f, respectively. Similar to normalized intensity and R images in Figure 2a and 2b, as-cast $I_{C=C}^{agg}$ and $I_{C=C}^{un}$ component frequency dispersion images show diffraction-limited features due to nanoscale phase segregation below the limit of our instrument resolution. Figure 4d shows the frequency dispersion of the $I_{C=C}^{agg}$ species for the annealed film, and comparison to normalized integrated intensity and R images in Figure 2d and 2e reveals similar features (i.e., blue circles, purple triangles, and brown squares). Regions represented by the blue circles likely correspond to partially aggregated P3HT chains, i.e., chains with increased interchain order (higher R values) but still possessing significant amounts of PCBM molecules. Purple triangles represent highly

aggregated or quasi-crystalline P3HT chains that show lower frequencies possibly due to increased conjugation lengths and appear as red areas in Figure 4d. This feature resembles characteristics observed in TEM and AFM images of P3HT/PCBM blend films that show distinct crystallite or 'nanowire' formation of P3HT chains. However, because the size scale of these features is usually on the order of tens of nanometers we cannot rule out the possibility of P3HT crystallite formation in solution, a common observation in several groups. Instead, it is more likely that these regions represent a statistical distribution of all possible crystallite types and orientations. We further consider the nature of aggregated species and their origins in more detail in the following.

Because the interfacial region between P3HT and PCBM represents an area of great importance due to photoinduced charge transfer at these boundaries, a detailed understanding of interfacial structural interactions is critical for developing improved material processing strategies for increased materials performance. The brown square in Figure 4d highlights an interfacial region that possesses a broad range of R values (1−4) likely due to competing intra- and interchain ordering effects. The larger R values probably arise from the fact that the two components are almost completely phase segregated or that the PCBM interactions at interfaces are folding P3HT chains differently in these regions. Further evidence for interfacial interactions can be observed from somewhat blue-shifted $I_{C=C}^{agg}$ frequencies in this region, as shown in Figure 4d.

Figure 4e shows the $I_{C=C}^{un}$ component of the annealed film that exhibits one noteworthy feature, namely, a region of lower frequency (red area) represented by the black diamond. Further comparison to Figure 2d and 2e for this same region suggests this is a PCBM-rich region with interpenetrating, randomly dispersed P3HT chains. These species represent unaggregated P3HT chains since high concentrations of PCBM effectively break up interchain interactions, which is further confirmed by their low R values (<1) and intensities. Lastly, comparison of as-cast and annealed $I_{C=C}^{agg}$ frequency dispersion histograms in Figure 4c and 4f shows a significant red shift in the latter ($\sim$4 cm^{-1}). It is tempting to assign this red shift to photoinduced charge transfer effects; however, this trend contradicts previous observations that annealing decreases the P3HT/PCBM interface area due to increased phase segregation that should lead to a reduction in charge transfer yields. This behavior is instead attributed to increased average conjugation lengths and intrachain order of P3HT in the annealed films. It is now interesting to consider the effects on R and frequencies of P3HT $I_{C=C}^{agg}$ and $I_{C=C}^{un}$ species when both P3HT/PCBM are allowed to fully phase segregate due to overannealing.

Although large improvements of P3HT/PCBM photovoltaic device efficiencies can result from annealing leading to increased intra- and interchain order of the P3HT component,[11,15,47] overannealing can lead to complete phase segregation of both components that diminishes material performance in a device environment. Figure 5 shows resonance Raman normalized intensity and R images of the C=C bands for thermally annealed P3HT/PCBM thin films cast from toluene (Figure 5a and 5b) and undoped P3HT thin films (Figure 5c and 5d). The overannealed blend film exhibits remarkable phase segregation with a well-resolved PCBM crystallite ($I \approx 0$), providing very high contrast between P3HT and PCBM components. Comparison of R values between overannealed blends and undoped P3HT films show approximately the same average values ($\sim$5.5), suggesting that no residual PCBM molecules exist within

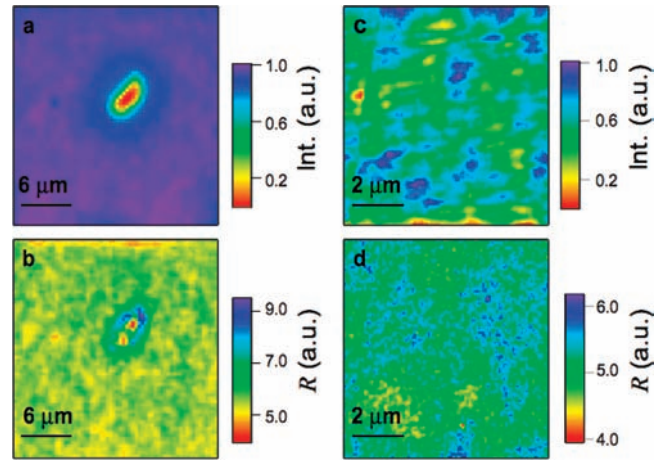

Figure 5. Normalized intensity and R images of "over-annealed" P3HT/PCBM blend thin films (a and b) and undoped annealed P3HT thin films (c and d).

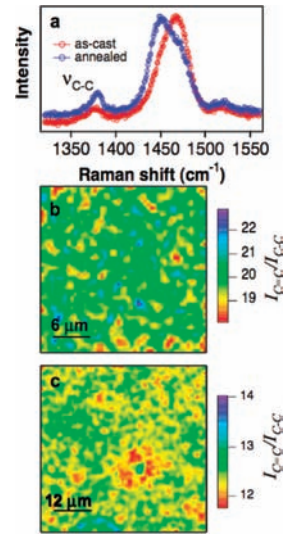

Figure 6. (a) Raman spectra of as-cast and annealed P3HT/PCBM thin films showing both the P3HT C=C and C−C symmetric stretching modes. Ratios of intensities of C=C/C−C modes for as-cast (b) and annealed (c) films for the same regions shown in Figures 2−4.

P3HT domains in blend films. Corresponding absorption spectra for overannealed blend films and undoped P3HT films show noticeable increases in aggregated/unaggregated (A^{agg}/A^{unagg}) ratios (1.6 and 1.4, respectively), which further confirms our conclusions from Raman spectroscopy and imaging results (see Supporting Information). On the basis of our observations from changes in Raman spectra and images upon annealing, it is apparent that significant structural rearrangements occur that lead to greater aggregation among P3HT molecules. We now consider the origins for the change in aggregation state of P3HT which are proposed to arise from a change in the planarity of P3HT chains.

Figure 6a shows typical Raman spectra of as-cast and annealed P3HT/PCBM films with the C−C symmetric stretching mode appearing at ca. 1380 cm^{-1}. Upon annealing, the relative intensity of the C−C mode increases substantially ($\sim$2×) with no change in frequency. By taking the ratio of the C=C and C−C total integrated intensities ($I_{C=C}/I_{C-C}$), we find that annealed films show an average value of $\sim$12 whereas as-cast films had an average value of $\sim$20. It is now informative to

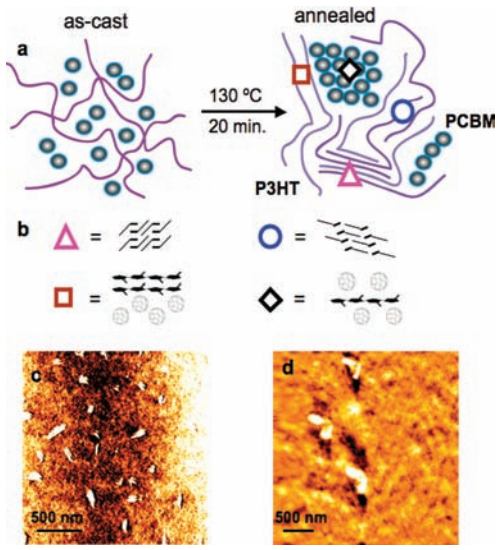

Figure 7. (a) Cartoon diagram of proposed P3HT (purple lines) and PCBM (gray circles) organization within blend thin films for as-cast and annealed systems. Symbols represent the four previously identified regions of the blend film showing intrinsic variation of P3HT intra- and interchain interactions due to the degree of PCBM phase segregation. (b) Proposed structures of regions, (purple triangles) "type 1" aggregates (average spacing ~3.8 Å):[49] (blue circles) "type 2" aggregates (average spacing ~4.47 Å),[49] (brown squares) interfacial P3HT, and (black diamonds) unaggregated P3HT. (c and d) AFM micrographs of as-cast and annealed P3HT/PCBM thin films.

construct spatial maps of $I_{C=C}/I_{C-C}$ values for as-cast and annealed films (Figure 6b and 6c, respectively) and compare these to *R* images shown in Figure 2. For annealed films, regions with larger *R* values correlate well with smaller $I_{C=C}/I_{C-C}$ ratios, whereas the larger $I_{C=C}/I_{C-C}$ values of as-cast films suggest a more twisted P3HT conformation and smaller *R* values. The relative increase in C−C mode intensities (decrease in $I_{C=C}/I_{C-C}$values) in annealed films is attributed to an increase of π electron density in C−C bonds resulting from an increase in planarity of P3HT chains. Previous Raman studies on oligothiophenes have suggested that the increase in C−C intensity is the result of increased charge transfer from C=C bonds;[48] however, very little experimental evidence exists to substantiate this claim. The relationship between C−C intensity and chain planarity is better observed by comparing Raman spectra from an oligothiophene derivative and P3HT annealed thin films that show larger C−C mode intensities in the latter presumably due to greater planarity (see Supporting Information). This observation is also consistent with recent experimental and theoretical studies of oligothiophenes that show planarity increases with increasing size (conjugation length).[35] Intuitively, the ability of P3HT chains to form cofacial $\pi-\pi$ stacks should be related to the degree of planarity; therefore, a direct correspondence between the degree of aggregation and planarity of P3HT chains is expected. The strong correlation between between *R* values and $I_{C=C}/I_{C-C}$ ratios discussed above suggests that these values do in fact provide a reliable means for tracking local changes in polymer chain planarity and, hence, aggregation. We now propose a scheme of materials organization which reconciles our data and observations with models obtained from X-ray crystallography and transmission electron microscopy.

Figure 7a shows a schematic diagram of proposed nano- to microscale organization of P3HT (purple lines) and PCBM (gray balls) components for as-cast and annealed blend films. AFM phase images are also shown in Figure 7c and 7d for as-cast and annealed films that exhibit phase segregation size scales of <100 nm and up to >1 μm, respectively, and rms surface roughness of <10 nm and up to ~50 nm, respectively. AFM micrographs also exhibit evidence for so-called P3HT nanowires recently reported in the literature[20,30] that correspond to highly aggregated P3HT chains in our Raman images (i.e., purple triangles, Figures 2 and 4). While AFM affords better lateral spatial resolution, it cannot report on morphology-dependent chemical structure changes arising from variations in intra- and interchain order and the relative DOS of aggregated/unaggregated species in complex blended systems. Using the notation of McCullough and co-workers, we attribute regions labeled by purple triangles ($R > 1.5$) as "type 1" P3HT that correspond to highly aggregated chains with an average *d* spacing of ~3.8 Å.[49] Regions labeled with blue circles are then assigned as "type 2" aggregates which have a slightly larger *d* spacing of 4.47 Å[49] and smaller *R* values ($1 < R < 1.5$). Figure 7b shows the structural schemes for these two types of aggregates. It is important to stress that our Raman approach does not provide the ability to resolve individual crystallites but rather regions with distributions of each type. In overannealed or undoped P3HT films, it is likely that most molecules are in the type 1 form, which is evident from the larger *R* values. Interestingly, P3HT chains near a PCBM interface exhibit distinctly different behavior from PCBM-poor regions. For example, brown squares highlight interfacial regions whereby P3HT molecules exhibit slightly higher frequencies possibly due to a disruption in interchain interactions, which is shown schematically in Figure 7b. However, *R* values still suggest a significant degree of aggregation which is reasonable due to increased phase segregation in these areas. Lastly, a small fraction of P3HT chains can remain imbedded in PCBM crystallites, which is represented by regions labeled by a black diamond. In this regime, interchain interactions do not exist, and therefore, the molecule should be in the unaggregated (solution-like) state. Because the P3HT structural properties vary significantly in the thin film, it is expected that the rates of important photovoltaic processes, such as charge transport, will also be strongly modulated by heterogeneity effects.

Future experiments will therefore involve resonance Raman imaging studies of the role of P3HT aggregation on photocurrent generation in functioning photovoltaic devices. On the basis of the results presented in this report, aggregated regions are expected to contribute more to observed current densities owing to the delocalized nature of these species that favors improved charge transport properties.[38] This new approach will allow further examination into the roles of aggregation effects on photocurrent generation that far surpass conventional photocurrent action spectroscopy measurements that instead average over the entire P3HT/PCBM active layer.

Conclusions

We have shown that the P3HT C=C symmetric stretching mode in P3HT/PCBM blend thin films consists of two distinct contributions from aggregated and unaggregated segments of P3HT. Aggregated ($I_{C=C}^{agg}$) species correspond to P3HT chains possessing high intra- and interchain order and long conjugation lengths, whereas unaggregated ($I_{C=C}^{un}$) species have less intra-

(48) Louarn, G.; Buisson, J. P.; Lefrant, S.; Fichou, D. *J. Phys. Chem.* **1995**, *99*, 11399–11404.

(49) Prosa, T. J.; Winokur, M. J.; McCullough, R. D. *Macromolecules* **1996**, *29*, 3654–3656.

and interchain order and shorter conjugation lengths. The relative concentrations, R, of these species also change with processing conditions from 0.79 ± 0.20 to 2.45 ± 0.77 for as-cast and annealed films, respectively, which is similar to observed changes of aggregated/unaggregated in optical absorption transitions. A direct relationship between the measured Raman R values and the relative DOS of these species is shown which is further corroborated by absorption spectra fitting procedures. The R values determined from resonance Raman spectroscopy, however, are expected to be a better estimate of the relative DOS than values obtained from absorption spectroscopy due to complications arising from Franck−Condon progressions (i.e., different Δ values for aggregated and unaggregated species) in the latter. By mapping morphology-dependent R values and $I_{C=C}^{agg}$ and $I_{C=C}^{un}$ frequency dispersion images for as-cast and annealed P3HT/PCBM films, we identify four regions corresponding to (1) PCBM-rich, unaggregated P3HT ($R < 1$), (2) interfacial P3HT ($R \approx 1-4$), (3) partially aggregated P3HT ($1 < R < 2$), and (4) highly aggregated/crystalline P3HT ($R > 2$). The origin of the change in aggregation state of P3HT is due to increased planarity of the chains that can be determined from intensity ratios of C═C/C−C stretching modes. Images of this parameter are strongly correlated with R images whereby smaller $I_{C=C}/I_{C-C}$ values (greater planarity) result in larger R values and therefore greater aggregation of P3HT chains. A simple model has also been proposed to explain these morphology-dependent features in terms of P3HT/PCBM packing characteristics supported by previous AFM, X-ray, and optical microscopic imaging reports. This information offers a new glimpse into the factors affecting the spatial variation of aggregation in P3HT that far surpasses the limited picture afforded from conventional ensemble absorption spectroscopy.

Acknowledgment. Financial support from UNM startup funds, Oak Ridge Associated Universities, and the Petroleum Research Fund (J.K.G.) is gratefully acknowledged. We thank Prof. Bradley Holliday (University of Texas, Austin) for providing oligothiophene samples for Raman studies.

Supporting Information Available: Photodegradation effects, dilute solution absorption spectra, comparison of pure component Raman spectra, effect of fit function for P3HT C═C line shape analysis, effect of initial guess for two-component Lorentzian line shape fits, effect of line width, and absorption line shape analysis for overannealed blend and pure P3HT thin films. This material is available free of charge via the Internet at http://pubs.acs.org.

JA900636Z